Ferroelectric Properties of $BaTi_{0.91}(Hf_{0.5}, Zr_{0.5})_{0.09}O_3$ Thin Films Fabricated by Pulsed Laser Deposition

Hirofumi KAKEMOTO,† Ken-ichi KAKIMOTO,†† Akira BABA, Shigetaka FUJITA and Yoichiro MASUDA

Department of Electrical and Electronic Engineering, Faculty of Engineering, Hachinohe Institute of Technology, 88-1, Ohbiraki, Myo, Hachinohe-shi, Aomori 031-8501

パルスレーザーデポジション法による $BaTi_{0.91}(Hf_{0.5}, Zr_{0.5})_{0.09}O_3$ 薄膜の作製と強誘電体特性

掛本博文† · 柿本健一†† · 馬場 明 · 藤田成隆 · 増田陽一郎

八戸工業大学工学部電気電子工学科，031-8501 青森県八戸市妙字大開 88-1

$BaTi_{0.91}(Hf_{0.5}, Zr_{0.5})_{0.09}O_3$ thin films were formed on Pt(111)/Ti/SiO_2/Si(100) substrates by pulsed laser deposition using fourth-harmonic-generated light ($\lambda = 266$ nm) of a Nd^{3+}:YAG laser beam. Crystallinity and stoichiometry of the thin films were determined by X-ray diffraction, X-ray fluorescence analysis and electron probe microanalysis. Their ferroelectric properties were investigated from electrical measurements. The leakage current density increased from 10^{-11} to 10^{-3} A·cm^{-2} with increasing electric field up to 200 kV·cm^{-1}. The dielectric constant, remanent polarization and coercive field of the $BaTi_{0.91}(Hf_{0.5}, Zr_{0.5})_{0.09}O_3$ thin films were estimated to be 120 at 1 kHz, 8.7 μC·cm^{-2} and 127 kV·cm^{-1}, respectively.

[Received January 23, 2001; Accepted May 23, 2001]

Key-words : *Ferroelectric thin films, $BaTi_{0.91}(Hf_{0.5}, Zr_{0.5})_{0.09}O_3$, Dielectric constant, D-E hysteresis loop*

1. Introduction

$BaTiO_3$ (BT) is a well-known fundamental ferroelectric perovskite oxide (ABO_3), and undergoes structural phase transitions at $T_{c1} = 130$°C, $T_{c2} = 5$°C and $T_{c3} = -80$°C. The ferroelectric properties at around T_{c2} are unstable because the temperature is close to room temperature (RT). Modification of the BT crystal structure has been considered to be a promising approach to improving the ferroelectric properties at RT.

By substituting a small proportion of the B(Ti)-site of BT with ($Hf_{0.5}$, $Zr_{0.5}$) cations, namely, a small addition of the dielectric phases $BaHfO_3$ and $BaZrO_3$ into BT, $BaTi_{0.91}(Hf_{0.5}, Zr_{0.5})_{0.09}O_3$ (soft BT, BTHZ-9) with a stable rhombohedral structure (C_{3v}, $a = b = c = 0.399$ nm, $\alpha = \beta = \gamma = 89.5°$) in a wide range of temperatures including RT was prepared.[1] BTHZ-9 shows a larger remanent polarization ($P_r = 15\ \mu C \cdot cm^{-2}$) and a smaller coercive electric field ($E_c = 0.35$ kV·cm^{-1}) than those of BT ($P_r = 7.0\ \mu C \cdot cm^{-2}$, $E_c = 3.5$ kV·cm^{-1}).[2] Therefore, BTHZ-9 thin film is promising has potential for electronic device applications, such as in ferroelectric random access memories (*FeRAMs*) and infrared sensors. Among various thin film deposition techniques, the pulsed laser deposition (PLD) method is expected to be a technique with one of the best control of film composition, even with slight amounts of constituent elements such as Hf and Zr as in this study. Using the PLD method, BTHZ-9 films were deposited on Pt(111)/Ti/SiO_2/Si(100) substrates in order to investigate the growth conditions and ferroelectric properties. Low O_2 partial pressure (10^{-3} Pa) was applied for *in situ* observation of BTHZ-9 thin film deposition by the reflection high-energy electron diffraction (RHEED) method.[3]

In this process, we report, in particular, the fabrication route of the films by the PLD method and the correlation between their stoichiometry and ferroelectric properties.

2. Experimental

The target materials used in the PLD technique were stoichiometric $BaTi_{0.91}(Hf_{0.5}, Zr_{0.5})_{0.09}O_3$ (BTHZ-9) and excess-Ba-containing $Ba_xTi_{0.91}(Hf_{0.5}, Zr_{0.5})_{0.09}O_3$ ($x = 1.5$, 3.0) materials, which were prepared from a mixture of $BaCO_3$ (Shin-Nihon Kagaku Co., purity: 99.7%), TiO_2 (Toho Titanium Co., purity: 99.94%), HfO_2 (Kantoh Kagaku Co., purity: 99.9%) and ZrO_2 (Daiichi Ki-Genso Co., purity: 99.98%). The powder mixtures were calcined at 1100°C for 2 h, and were pressed into disks (20 mm in diameter and 2 mm in thickness) which were sintered at 1350°C for 3 h.

The Pt(111)/Ti/SiO_2/Si(100) substrates were selected for BTHZ-9 film deposition. The substrates were heated to 600°C (T_s) in a vacuum chamber with an oxygen partial pressure lower than 10^{-3} Pa. The light source for PLD was fourth-harmonic-generation (FHG light, $\lambda = 266$ nm) from double nonlinear optical crystals (KDP: KH_2PO_4) of a Nd^{3+}:YAG laser beam (Spectron Laser System, SL850; $\lambda = 1064$ nm). The FHG light with power density of 1.2 J·cm^{-2} was focused onto the BTHZ-9 target, and its repetition frequency of irradiation was kept at 10 Hz during deposition. The film thickness was about 700 nm. The deposited films were subsequently annealed at 800°C for 1 h under O_2 atmosphere (1.96×10^5 Pa) in order to enhance crystallinity and reduce O_2 vacancies.[4] The growth conditions of various BTHZ-9 thin films are listed in Table 1.

The crystallinity and stoichiometry of samples were characterized by X-ray diffraction (XRD, Rigaku-Denki

† Now with Department of Inorganic Materials, Faculty of Engineering, Tokyo Institute of Technology, 2-12-1, Ookayama, Meguro-ku, Tokyo 152-8552
現在：東京工業大学大学院理工学研究科，152-8552 東京都目黒区大岡山 2-12-1

†† Now with Department of Material Science and Engineering, Faculty of Engineering, Nagoya Institute of Technology, Gokiso-cho, Showa-ku, Nagoya-shi 466-8555
現在：名古屋工業大学工学部材料工学科，466-8555 愛知県名古屋市昭和区御器所町

Table 1. Growth Conditions of $BaTi_{0.91}(Hf_{0.5}, Zr_{0.5})_{0.09}O_3$ Thin Film on $Pt/SiO_2/Si(100)$ Substrate Prepared by Pulsed Laser Deposition. x Indicates Ba Content in $Ba_xTi_{0.91}(Hf_{0.5}, Zr_{0.5})_{0.09}O_3$

Sample	x	T_s (°C)	rep.(Hz)
Sample A	1.0	600	10
Sample B	3.0	600	10
Sample C	1.0 and 3.0	600	10
Sample D	1.5	600	10

RAD-3c), X-ray fluorescence (XRF; Rigaku-Denki Co., type 3030) analysis and electron probe microanalysis (EPMA; JEOL, JXA-8800R). The upper electrodes (Pt, circular dots, 0.3 mm in diameter, 0.071 mm^2 in area) were deposited onto BTHZ-9 film by RF sputtering using a shadow mask. The ferroelectric properties of the thin film were evaluated by measuring the leakage current density (i). The frequency dependence of the dielectric constant (ε_r) was calculated from the capacitance obtained using a LCR meter (Hewlett-Packard 4284A). The D-E hysteresis loop was observed using a Sawyer-Tower circuit.

3. Results and discussion

Figure 1 shows the XRD patterns of BTHZ-9 thin films on $Pt(111)/Ti/SiO_2/Si(100)$ substrates fabricated by the PLD method. Sample A was prepared from the stoichiometric BTHZ-9 target, and its XRD pattern indicates a perovskite structure. However, only a slight amount of Ba was detected by XRF analysis, indicating massive Ba loss during the PLD process. Sample B does not show a perovskite structure, although the Ba content in the target was enhanced compared to sample A. The peak at $2\theta = 20°$ is attributed to segregated BaO and/or TiO_2-related compounds, implying that excessive Ba content does not allow BTHZ-9 to form a perovskite structure.

Based on these results, sample C was prepared by combinating stoichiometric and excess-Ba ($x = 3.0$) BTHZ-9 targets. Thin films were deposited alternately from the two targets in order to form multilayers with 8 layers. Furthermore, O_2 annealing was carried out after PLD in order to enhance alternate diffusion of Ba and Ti and to reduce O_2 vacancies in the film. Sample C presents a strong [001] orientation of the perovskite structure, although segregated compounds are still indicated by the XRD pattern. The Pb(Zr, Ti)O_3 film on the $Pt(111)/Ti/SiO_2/Si(100)$ substrate prepared by PLD shows preferential [111] orientation. The crystal orientation is varied by changing the induced partial O_2 pressure during deposition.[5),6)] On the other hand, BT-related film usually shows a preferential [001] orientation. The crystal orientation of BT-related film is not strongly influenced by $Pt(111)/Ti/SiO_2/Si(100)$ or induced partial O_2 pressure during deposition.[7)] In this case, BTHZ-9 also shows a preferential [001] orientation. This is a result of the self-growth and orientation of BTHZ-9 grains. The lattice parameter of sample C was calculated to be $a = 0.399$ nm. Sample D was prepared from a $Ba_{1.5}Ti_{0.91}(Hf_{0.5}, Zr_{0.5})_{0.09}O_3$ target. Its XRD pattern indicates a well-developed perovskite structure with only a slight amount of segregated compounds.

Figure 2 shows the distribution map of Ba and O elements obtained by EPMA for the as-deposited sample A and annealed sample D. A weak Ba pattern is observed in Fig. 2 (a) for sample A. On the other hand, sample D shows a much higher. These results are also supported by the results

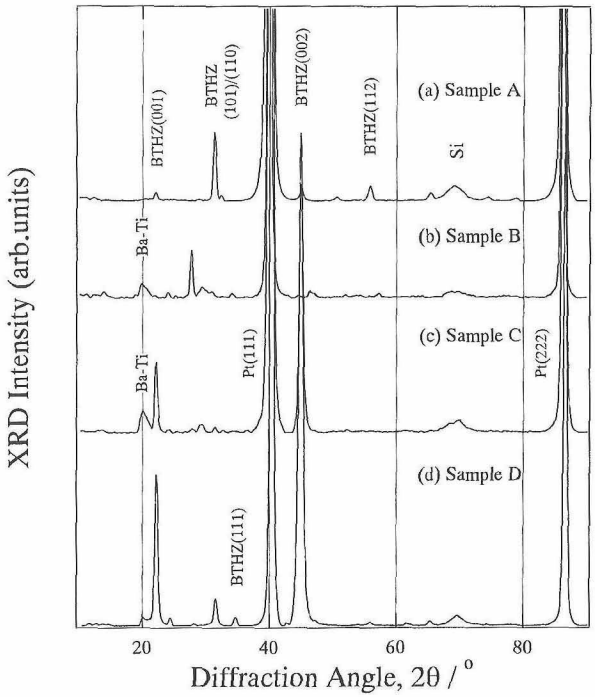

Fig. 1. XRD patterns of BTHZ-9 thin films on $Pt(111)/Ti/SiO_2/Si(100)$ substrates fabricated by pulsed laser deposition using various $Ba_xTi_{0.91}(Hf_{0.5}, Zr_{0.5})_{0.09}O_3$ ($x = 1.0$, 1.5, 3.0) targets.

of XRF analysis of samples A and D. The excess-Ba target was needed for the preparation of stoichiometric BTHZ-9 thin film under low O_2 partial pressure during the PLD process in order to enable *in situ* observation of film growth by RHEED. To evaluate the electrical conductivity of the samples, leakage current density (i) was measured under an applied electric field (E) of up to 200 $kV \cdot cm^{-1}$ (i-E property). Samples A and B showed metallic conductive behaviors. In contrast, samples C and D presented dielectric behaviors. The Ti/Hf/Zr ratio of BTHZ-9 film is estimated to be 0.91/0.045/0.045.

Figure 3 shows the logarithmic plot of the i-E relationship for sample D. The inset in Fig. 3 shows the linear plot of the i-E relationship for sample D. The value of i increases abruptly from 10^{-11} to 10^{-3} $A \cdot cm^{-2}$ with increasing E up to 200 $kV \cdot cm^{-1}$. In order to characterize the electrical conductivity at the interfaces between the BTHZ-9 thin film and electrodes, the i curve was analyzed using the formula $i = C'E^n$, where C' is a constant and n is an exponential index. The applied electric field during measurement was swept at 245.7 $V \cdot cm^{-1} \cdot s$. As shown in the inset, n was estimated to be 1.0 below 100 $kV \cdot cm^{-1}$, i.e., the Ohmic property i-E, n

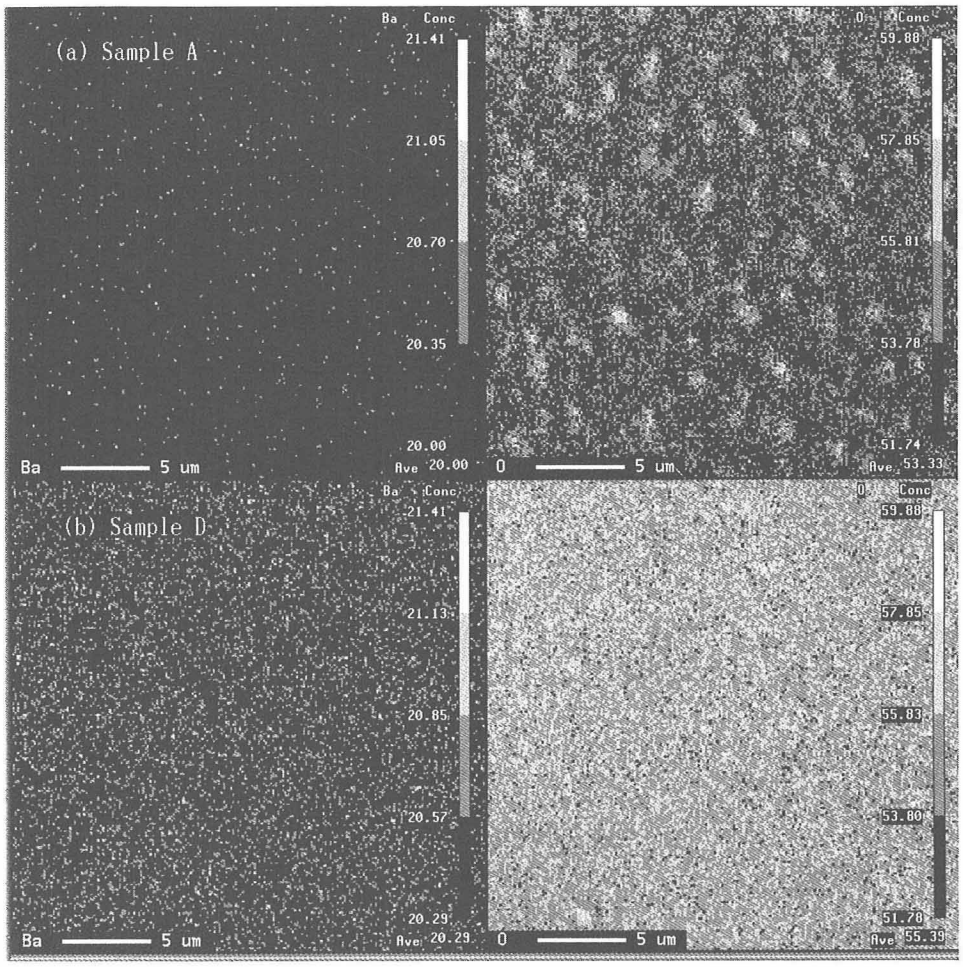

Fig. 2. Ba and O distribution maps for BTHZ-9 thin films of (a) sample A and (b) sample D, obtained by EPMA.

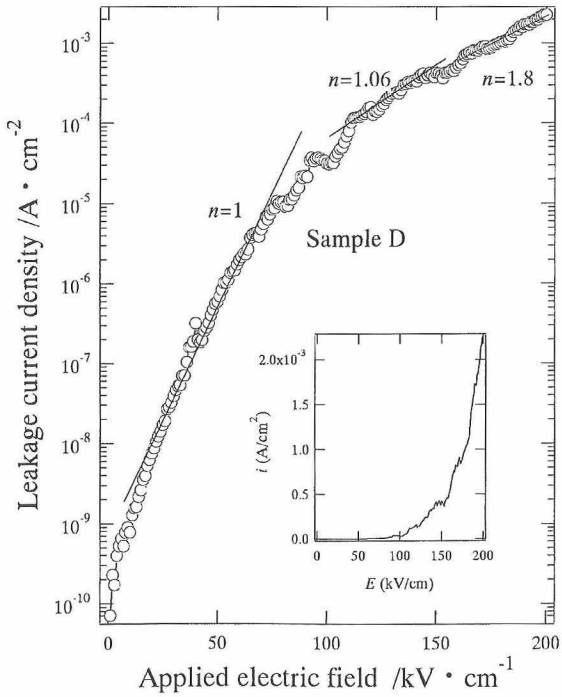

Fig. 3. Leakage current density of sample D. The i–E property shows dielectric conduction.

$=1.06$ between 100 and 150 kV·cm^{-1}, and $n=1.8$ between 150 and 200 kV·cm^{-1}. Finally the i curve increased exponentially above 200 kV·cm^{-1}. These results can be explained in terms of the generated space charge current between the ferroelectric film and electrodes.[4]

Figure 4(a) shows the frequency (f) dependence of ε_r and dielectric loss ($\tan\delta$) for sample C. ε_r and $\tan\delta$ are measured as 53 and 0.125 at 1 kHz, respectively. This ε_r value is relatively low. The dielectric properties of a BT polycrystal, BT single crystal and BT thin film have been reported.[2),8),9)] The BT polycrystal exhibits large ε_r because of random orientation. The ε_r values of the BT single crystal along the a- and b-axes are also large. ε_r along the c-axis is, however, smaller than along other axes. Therefore, relatively low ε_r seems to correlate with the crystal orientation of sample C (grown along the c-axis), and is consistent with the results for the BT thin film prepared by PLD reported in Ref. 9). In addition, ε_r of sample C abruptly decreased with increasing f, which is thought to be due to a secondary phase with a low ε_r. Figure 4(b) shows a schematic illustration of the proposed grain growth model of sample C during O_2 annealing. The excess Ba segregates from BTHZ-9 grains, based on the phase diagram of BT. This excess Ba may react with Ti-rich regions in BTHZ-9 complex phases, as indicated by the XRD pattern. Following these processes, sample C may contain complex phases other than perovskite phases. These grains are considered to form direct ($1/C_s = 1/C_0 + 1/C_f + 1/C_1$) and parallel ($C_s = C_0 + C_f + C_1$) capaci-

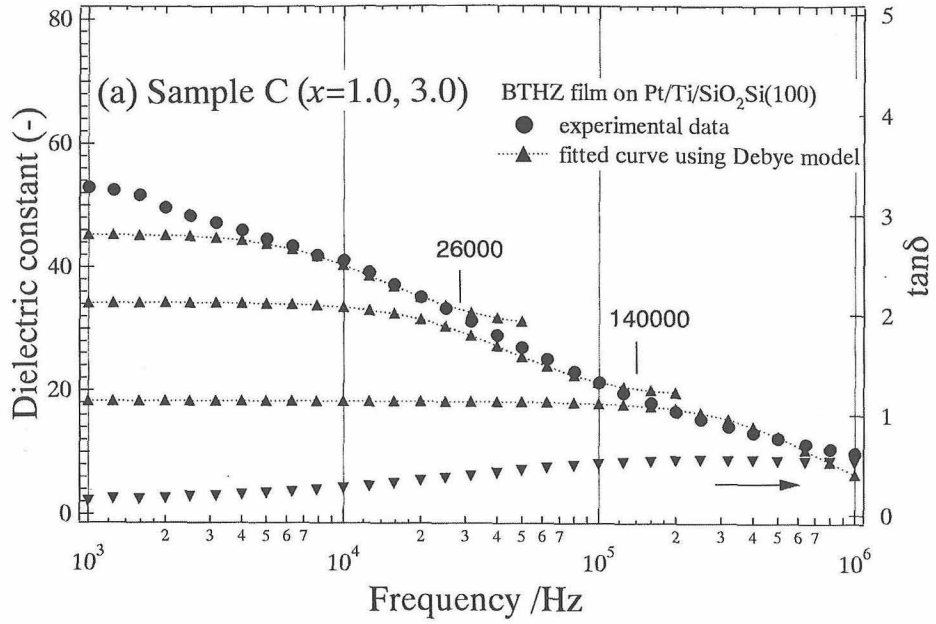

(b) Grain growth model

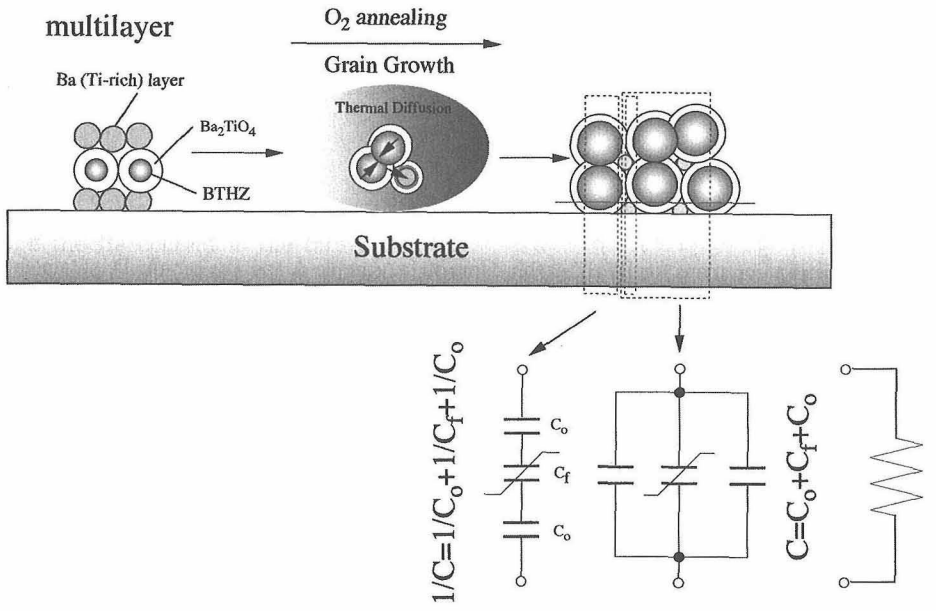

Fig. 4. (a) Frequency dependence of dielectric constant and tan δ for sample C and (b) its grain growth model during O_2 annealing.

tors in the microstructure, where C_s is the measured capacitance of sample C, C_0 and C_1 are low dielectric phase capacitors, and C_f is a ferroelectric phase capacitor.

The ε_r values shown in Fig. 4(a) decrease in 3 steps with increasing f. On the other hand, tan δ increases with increasing f. Accordingly, the ε_r spectrum consists of 3 dielectric functions. It is noted that a parallel factor ($\varepsilon_s=\varepsilon_0+\varepsilon_f+\varepsilon_1$) is observed in sample C. In order to calculate the dielectric and relaxation constants for the ferroelectric phase in sample C, we introduced the Debye model represented by $\varepsilon_r=\varepsilon_{r\infty}+(\varepsilon_{r0}-\varepsilon_{r\infty})/(1+\omega^2\tau^2)$, where ε_{r0} is the dielectric constant at low frequency, $\varepsilon_{r\infty}$ is the dielectric constant in the infrared region, ω is angular frequency ($\omega=2\pi f$), and τ is the relaxation constant. The ε_r curves shown in Fig. 4(a) were analyzed by fitting this Debye model. As a result, the τ value for the ferroelectric phase in the lowest fitted curve was obtained as 2.14×10^{-6} s. This value is consistent with the relaxation time of ferroelectric material.

Figure 5 shows the f dependence of ε_r and tan δ for sample D. ε_r and tan δ gradually decrease with increasing f. ε_r and tan δ are measured as 120 and 0.15 at 1 kHz in Fig. 5, respectively. ε_r of sample D synthesized using the $Ba_{1.5}Ti_{0.91}(Hf_{0.5}, Zr_{0.5})_{0.09}O_3$ target gradually decreased with increasing frequency, and its relaxation constant in the Debye model was revealed to be undistributed. These superior properties compared to those of sample C may indicate that sample D consist of a single ferroelectric BTHZ-9 phase. Figure 6 shows the D–E hysteresis loops of sample D. The remanent polarization (P_r) and coercive field (E_c) are estimated to be 8.7 $\mu C\cdot cm^{-2}$ and 127 $kV\cdot cm^{-1}$, respectively.

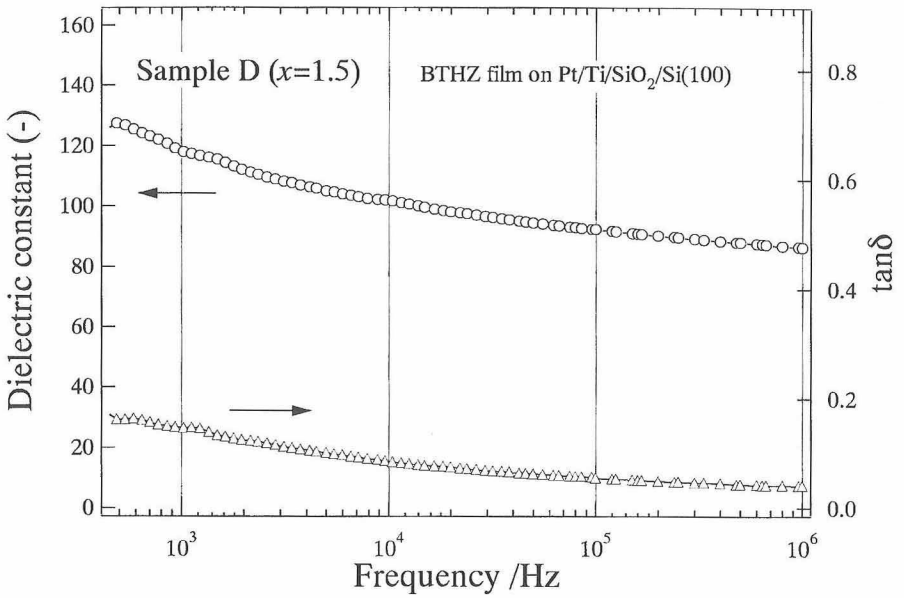

Fig. 5. Frequency dependence of dielectric constant and tan δ for sample D.

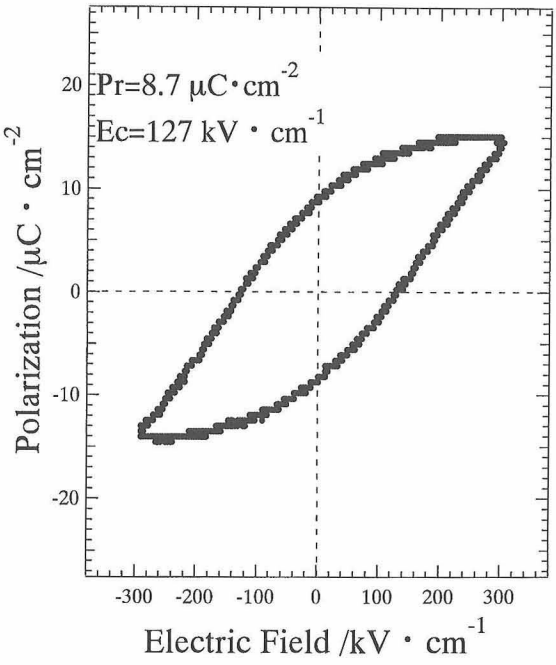

Fig. 6. *D–E* hysteresis loop for sample D observed at an applied electric field of 300 kV·cm^{-1}.

This P_r value is larger than that of BT bulk ($P_r=7.0\,\mu C\cdot cm^{-2}$).[9]

4. Conclusions

Several kinds of $Ba_xTi_{0.91}(Hf_{0.5}, Zr_{0.5})_{0.09}O_3$ films were prepared on Pt(111)/Ti/SiO_2/Si substrates by pulsed laser deposition using stoichiometric, excess-Ba and multicomposition targets. The film prepared from the $Ba_{1.5}Ti_{0.91}(Hf_{0.5}, Zr_{0.5})_{0.09}O_3$ target showed dielectric behavior of the leakage current density against applied electric field. The dielectric constant of a multilayered sample abruptly decreased with increasing applied frequency, which is thought to be due to a secondary phase with a low dielectric constant. The relaxation constant for the ferroelectric phase was calculated by curve fitting using the Debye model. The dielectric constant of the sample synthesized using the $Ba_{1.5}Ti_{0.91}(Hf_{0.5}, Zr_{0.5})_{0.09}O_3$ target gradually decreased with increasing frequency, and its relaxation constant in the Debye model was revealed to be undistributed.

The *D–E* hysteresis loop of the sample synthesized from the $Ba_{1.5}Ti_{0.91}(Hf_{0.5}, Zr_{0.5})_{0.09}O_3$ target was observed at an applied electric field of 300 kV·cm^{-1}. The remanent polarization and coercive field were estimated to be 8.7 μC·cm^{-2} and 127 kV·cm^{-1}, respectively. This remanent polarization is larger than that of $BaTiO_3$ ceramics ($P_r=7.0\,\mu C\cdot cm^{-2}$), and is caused by the $BaTi_{0.91}(Hf_{0.5}, Zr_{0.5})_{0.09}O_3$ phase.

Acknowledgments This work was supported by Next Generation of Research for the Future, Japan Society for the Promotion of Science (JSPS-RFTF 96P00105). The author would like to thank Takeyo Tsukamoto for useful discussion.

References

1) Setter, N. and Colla, E. L., "Ferroelectric Ceramics," Birkhauser Verlag, Basel-Boston-Berlin (1993) p. 325.
2) Thongrueng, J., Tsuchiya, T., Masuda, Y., Fujita, S. and Nagata, K., *Jpn. J. Appl. Phys.*, **38**, 5309–13 (1999).
3) Kakemoto, H., Fujita, S. and Masuda, Y., *Jpn. J. Appl. Phys.*, **39**, 5374–78 (2000).
4) Masuda, Y., Fujita, S., Nishida, T., Masumoto, H. and Hirai, T., Proc. of the 11th IEEE Int. Symp. Applications of Ferroelectrics, Switzerland (1998), IEE, Switzerland (1998) pp. 23–25.
5) Wang, Z. J., Kikuchi, K. and Maeda, R., *Jpn. J. Appl. Phys.*, **39**, 5413–17 (2000).
6) Kakimoto, K., Kakemoto, H. and Masuda, Y., *J. Ceram. Soc. Japan*, **109**, 149–54 (2001).
7) Jang, J. W., Kim, Y. H., Hahn, T. S., Choi, S. S. and Chung, S. J., *Jpn. J. Appl. Phys.*, **35**, L699–702 (1996), Kamehara, N., Tsukada, M., Cross, J. S. and Kurihara, K., *J. Ceram. Soc. Japan*, **105**, 746–50 (1997).
8) Jona, F. and Shirane, G., "Ferroelectric Crystals," Dover Pub., New York (1993) p. 111.
9) Roy, D. and Krupanidhi, S. B., *Appl. Phys. Lett.*, **61**, 2057–59 (1992).